Dynamic Instability of Sandwich Plates

Rita Alves Baía dos Santos
ritabaiasantos@tecnico.ulisboa.pt

Instituto Superior Técnico, Universidade de Lisboa, Portugal

December 2022

Abstract

This work presents the development of a model to analyse the dynamic instability of composite plates, including sandwich plates. Two models to analyse isotropic, orthotropic and laminated composite plates were developed in Matlab. These models are based on the first-order shear deformation theory (FSDT) and the higher-order shear deformation theory (HSDT). These formulations are then used to model a sandwich plate. Using a mixed layer-wise approach, the core is modelled with the HSDT and the face sheets use the FSDT. The finite element model applies an eight-node serendipity quadratic element. A free vibration analysis was performed in order to validate the formulation of the mass and stiffness matrices. Later on, the dynamic instability regions for isotropic, orthotropic, laminated composite and sandwich plates is studied. A special case of sandwich plates, when its core is made of viscoelastic materials, is, also, study.
Keywords: Sandwich Plates, Laminated Composite Plates, Dynamic Instability, FSDT, HSDT

1. Introduction

Composite materials are obtained by combining two or more materials that together provide properties that are normally not achieved individually, at a reasonable cost [1]. A sandwich panel is a composite material consisting of two thin laminate skins and a lightweight, thick core structure. Despite the thickness of the core, sandwich composites are lightweight and have relatively high flexural strength [2]. Then sandwich plates are increasingly utilised in the construction of different structures in multiple engineering applications, due to their high strength and stiffness, low weight, high durability and ease of manufacturing [3].

It is possible to improve even more the properties of sandwich plates making the core with a viscoelastic material. Usually this material is a damping material that presents great stress recovery, relaxation and creep. That means that when the applied stress is removed, some of the stresses created in the material during the recovery period are eliminated immediately and the residual stress slowly tends to zero. This technique is interesting for different aspects, such as, vibration and noise control, due to their ability to dissipate energy [4].

Structural members of any engineering application are subjected to different kinds of loads and excitations, sometimes those loads can be dynamic, periodic or not, and is essentially to study their effects on the structural behaviour. Some combination of loads can lead to dynamic instability. So it is fundamental to study the static and dynamic stability behaviour of the structural members in the design of their components [5].

The finite element models to be used and developed in this work are based on the models developed by Araújo et al. [6] for dynamic analysis and extended to buckling analysis by Tomé [7].

2. Development of Plates Elements

A laminate is an assembly of more than one lamina stacked in order to obtain a structure with the desired thickness and stiffness. While, a lamina or ply is a sheet of composite material. Each lamina can be made of an isotropic or orthotropic material.

An orthotropic material has three mutually orthogonal planes of material symmetry.

If the coordinate planes are chosen parallel to the three orthogonal planes of symmetry, that is, the principal material directions (x_1, x_2), the stress-strain relations can be given by:

$$\begin{Bmatrix} \sigma_{11} \\ \sigma_{22} \\ \sigma_{33} \\ \sigma_{23} \\ \sigma_{13} \\ \sigma_{12} \end{Bmatrix} = \begin{bmatrix} \frac{1}{E_1} & -\frac{\nu_{21}}{E_2} & -\frac{\nu_{31}}{E_3} & 0 & 0 & 0 \\ -\frac{\nu_{12}}{E_1} & \frac{1}{E_2} & -\frac{\nu_{32}}{E_3} & 0 & 0 & 0 \\ -\frac{\nu_{13}}{E_1} & -\frac{\nu_{23}}{E_2} & \frac{1}{E_3} & 0 & 0 & 0 \\ 0 & 0 & 0 & \frac{1}{G_{23}} & 0 & 0 \\ 0 & 0 & 0 & 0 & \frac{1}{G_{13}} & 0 \\ 0 & 0 & 0 & 0 & 0 & \frac{1}{G_{12}} \end{bmatrix}^{-1} \begin{Bmatrix} \varepsilon_{11} \\ \varepsilon_{22} \\ \varepsilon_{33} \\ \varepsilon_{23} \\ \varepsilon_{13} \\ \varepsilon_{12} \end{Bmatrix} \quad (1)$$

An isotropic material presents an infinite number of planes of material symmetry, which means that each material property is independent of the direction. The properties are related as following:

$$G = \frac{E}{2\,(1+\nu)} \quad (2)$$

2.1. Laminate Theories

Equivalente single layer (ESL) theories reduce a 3D problem to a 2D problem by making suitable assumptions regarding the kinematics of deformation or the stress state through the thickness. This will allow to reduce the computational effort and the complexity of the problem without losing relevant accuracy. This happens because by taking into account the Cartesian coordinate system at the mid-surface of the entire structure, models based on similar single layer plate theories are created, and the deformation of the plate is described in terms of the characteristics of this reference plane. Because of this, the overall number of degrees of freedom is independent of the number of plies. HSDT and FSDT are the ESL theories that are going to be used in this work.

Regarding the displacement field, the FSDT considers:

$$u(x,y,z,t) = u_0(x,y,t) + z\theta_x(x,y,t) \tag{3a}$$

$$v(x,y,z,t) = v_0(x,y,t) + z\theta_y(x,y,t) \tag{3b}$$

$$w(x,y,z,t) = w_0(x,y,t) \tag{3c}$$

where θ_x and θ_y are the rotation of a transverse normal about the y and x axis, respectively.

For the HSDT the displacement field is written as:

$$u(x,y,z,t) = u_0(x,y,t) + z\theta_x(x,y,t) + z^2u_0^*(x,y,t) + z^3\theta_x^*(x,y,t) \tag{4a}$$

$$v(x,y,z,t) = v_0(x,y,t) + z\theta_y(x,y,t) + z^2v_0^*(x,y,t) + z^3\theta_y^*(x,y,t) \tag{4b}$$

$$w(x,y,z,t) = w_0(x,y,t) + z\theta_z(x,y,t) + z^2w_0^*(x,y,t) \tag{4c}$$

where u_0^*, v_0^*, w_0^*, θ_x^*, θ_y^* and θ_z are higher order terms in the series expansion to be determined.

2.2. Finite Element Model

Two finite element models (FEM) are developed, since this work focus on two models for laminate theories. The models presented use an eight-node serendipity quadratic element. Each node has 5 and 11 degrees of freedom for the FSDT and HSDT, respectively. The shape functions for each element are given by equation (5), where ξ and η are the natural coordinates of the element.

$$\{N^e\} = \begin{Bmatrix} N_1^e \\ N_2^e \\ N_3^e \\ N_4^e \\ N_5^e \\ N_6^e \\ N_7^e \\ N_8^e \end{Bmatrix} = \begin{Bmatrix} \frac{1}{4}(1-\xi)(1-\eta)(-\xi-\eta-1) \\ \frac{1}{4}(1+\xi)(1-\eta)(\xi-\eta-1) \\ \frac{1}{4}(1+\xi)(1+\eta)(\xi+\eta-1) \\ \frac{1}{4}(1-\xi)(1+\eta)(-\xi+\eta-1) \\ \frac{1}{2}(1-\xi^2)(1-\eta) \\ \frac{1}{2}(1+\xi)(1-\eta^2) \\ \frac{1}{2}(1-\xi^2)(1+\eta) \\ \frac{1}{2}(1-\xi)(1-\eta^2) \end{Bmatrix} \tag{5}$$

Mass Matrix

The mass matrix can be obtained by:

$$[M^e] = \int_A [N]^T [P] [N] \, dA \tag{6}$$

where A is the in-plane area of the plate and $[P]$ is obtained by:

$$[P] = \int_{-h/2}^{h/2} \rho [Z]^T [Z] \, dz \tag{7}$$

where $[Z]$ depends on which model is being used, and is given by:

$$[Z]_{FSDT} = \begin{bmatrix} 1 & 0 & 0 & z & 0 \\ 0 & 1 & 0 & 0 & z \\ 0 & 0 & 1 & 0 & 0 \end{bmatrix} \tag{8a}$$

$$[Z]_{HSDT} = \begin{bmatrix} 1 & 0 & 0 & z & 0 & 0 & z^2 & 0 & 0 & z^3 & 0 \\ 0 & 1 & 0 & 0 & z & 0 & 0 & z^2 & 0 & 0 & z^3 \\ 0 & 0 & 1 & 0 & 0 & z & 0 & 0 & z^2 & 0 & 0 \end{bmatrix} \tag{8b}$$

Changing coordinates from (x, y) to the natural coordinates (ξ, η) the element mass matrix is given by:

$$[M^e] = \int_{-1}^{+1} \int_{-1}^{+1} \left([N]^T [P] [N] \right) \det(J) \, d\xi \, d\eta \tag{9}$$

Linear Stiffness Matrix

The element linear stiffness matrix $[K^e]$ is obtained by:

$$[K^e] = \int_{-1}^{+1} \int_{-1}^{+1} \left([B_m]^T [D_m] [B_m] + [B_m]^T [D_c] [B_b] + [B_b]^T [D_c] [B_m] + [B_b]^T [D_c] [B_b] + [B_s]^T [D_s] [B_s] \right) \det(J) \, d\xi \, d\eta \tag{10}$$

Geometric Stiffness Matrix

The element geometric stiffness matrix $[K_G^e]$ can be calculated by:

$$[K_G^e] = \int_{-1}^{+1} \int_{-1}^{+1} \left([G]^T [\tau] [G] \right) \det(J) \, d\xi \, d\eta \tag{11}$$

2.3. Vibration Analysis

Performing the eigenvalue problem shown on equation (12), on a structure, the free vibration frequencies can be obtained. Where ω is the free vibration frequency.

$$\left| [K] - \omega^2 [M] \right| = 0 \tag{12}$$

The boundary conditions that the plates were under during all analysis in this work were the same for all the models presented. The plates are simply supported in all the four edges.

A vibration analysis was performed in an isotropic square plate with only a ply, with $a = b = 0.3$m, thickness of 0.003m and $\nu = 0.25$. The results obtained for the first mode (1,1) are shown in Table 1. Important to mention that the results presented are non dimensional given by $\bar{\omega} = \omega a^2 \sqrt{\frac{\rho h}{D}}$ with $D = \frac{Eh^3}{12(1-\nu^2)}$.

The theoretical results presented were calculated by [8]:

$$\omega = \sqrt{\frac{D}{\rho h}} \left[\left(\frac{m}{a} \right)^2 + \left(\frac{n}{b} \right)^2 \right] \pi^2 \tag{13}$$

Table 1: Non dimensional free vibration frequency results for an isotropic square plate

$N \times N$	$\bar{\omega}$ FSDT	$\bar{\omega}$ HSDT	$\bar{\omega}$ Theoretical	Relative error (FSDT)	Relative error (HSDT)
2x2	33.1171	33.7461	19.739	67.775%	70.962%
5x5	19.7615	19.7662	19.739	0.114%	0.138%
10x10	19.7328	19.7329	19.739	0.031%	0.031%
15x15	19.7325	19.7325	19.739	0.033%	0.033%
20x20	19.7324	19.7324	19.739	0.033%	0.033%

Table 1 shows that the results obtained, for both FSDT and HSDT, converge after a mesh size of 10×10. After convergence is accomplished, the relative error of the free vibration frequencies, for both FSDT and HSDT models, are lower than 1% for all modes studied.

From this analysis it is possible to validate the formulations done for the mass matrix and linear stiffness matrix, for both FSDT and HSDT models.

3. Dynamic Instability Analysis

To find the regions of dynamic instability of a structure it is useful to use the theory of systems of Mathieu-Hill differential equations with periodic coefficients. Analysing the structures studied in this work its equations of motions can be presented in the Mathieu-Hill equation form as following:

$$[M]\{\ddot{x}\} + [K]\{x\} - P(t)[K_G]\{x\} = 0 \qquad (14)$$

where $[M]$, $[K]$ and $[K_G]$ are, respectively, the mass matrix, the stiffness matrix and the geometric stiffness matrix. $P(t)$ is the periodic force that can be presented as $P(t) = P_S + P_d \cos(\theta t)$. P_S is the static component and P_d is the dynamic component of the applied load.

The method suggested by Bolotin [9] was used to determine the regions of dynamic instability. The boundaries between the dynamic stability and instability regions are characterised by periodic solutions with period T and 2T in equation (14). These solutions can be expanded into Fourier series. Periodic solutions with period 2T and T in equation (14) present, respectively, the form shown on equations (15) and (16).

$$x(t) = \sum_{k=1,3,5}^{\infty} a_k \sin\frac{k\theta t}{2} + b_k \cos\frac{k\theta t}{2} \qquad (15)$$

$$x(t) = b_0 + \sum_{k=2,4,6}^{\infty} a_k \sin\frac{k\theta t}{2} + b_k \cos\frac{k\theta t}{2} \qquad (16)$$

Substituting (15) or (16) in equation (14) and equating the coefficients of identical $\sin\frac{k\theta t}{2}$ and $\cos\frac{k\theta t}{2}$ a system of linear homogeneous algebraic equations are obtained with infinite equations and infinite unknowns a_k and b_k. The system of linear homogeneous equations has non-zero solutions only if the determinant of the coefficients of the system is equal to zero. The equations of boundary frequencies are then obtained from the condition that equation (14) presents periodic solutions if the obtained determinants of the homogeneous systems are zero.

Equation (17) is the equation of boundary frequencies that allows to find the regions of instability which boundaries are the periodic solutions with a period 2T. For the regions of instability bounded by the periodic solutions with a period T, the equations of boundary frequencies are equations (18a) and (18b), where θ is the frequency of the external load and [I] is the identity matrix.

$$\begin{vmatrix} [I] - (P_S \pm \frac{P_d}{2})[K]^{-1}[K_G] - \frac{\theta^2}{4}[K]^{-1}[M] & -\frac{P_d}{2}[K]^{-1}[K_G] & 0 & \dots \\ -\frac{P_d}{2}[K]^{-1}[K_G] & [I] - P_S[K]^{-1}[K_G] - \frac{9\theta^2}{4}[K]^{-1}[M] & -\frac{P_d}{2}[K]^{-1}[K_G] & \dots \\ 0 & -\frac{P_d}{2}[K]^{-1}[K_G] & [I] - P_S[K]^{-1}[K_G] - \frac{25\theta^2}{4}[K]^{-1}[M] & \dots \\ \dots & \dots & \dots & \dots \end{vmatrix} = 0 \qquad (17)$$

$$\begin{vmatrix} [I] - P_S[K]^{-1}[K_G] - \theta^2[K]^{-1}[M] & -\frac{P_d}{2}[K]^{-1}[K_G] & 0 & \dots \\ -\frac{P_d}{2}[K]^{-1}[K_G] & [I] - P_S[K]^{-1}[K_G] - 4\theta^2[K]^{-1}[M] & -\frac{P_d}{2}[K]^{-1}[K_G] & \dots \\ 0 & -\frac{P_d}{2}[K]^{-1}[K_G] & [I] - P_S[K]^{-1}[K_G] - 9\theta^2[K]^{-1}[M] & \dots \\ \dots & \dots & \dots & \dots \end{vmatrix} = 0 \qquad (18a)$$

$$\begin{vmatrix} [I] - P_S[K]^{-1}[K_G] & -\frac{P_d}{2}[K]^{-1}[K_G] & 0 & 0 & \dots \\ -P_d[K]^{-1}[K_G] & [I] - P_S[K]^{-1}[K_G] - \theta^2[K]^{-1}[M] & -\frac{P_d}{2}[K]^{-1}[K_G] & 0 & \dots \\ 0 & -\frac{P_d}{2}[K]^{-1}[K_G] & [I] - P_S[K]^{-1}[K_G] - 4\theta^2[K]^{-1}[M] & -\frac{P_d}{2}[K]^{-1}[K_G] & \dots \\ 0 & 0 & -\frac{P_d}{2}[K]^{-1}[K_G] & [I] - P_S[K]^{-1}[K_G] - 9\theta^2[K]^{-1}[M] & \dots \\ \dots & \dots & \dots & \dots & \dots \end{vmatrix} = 0 \qquad (18b)$$

From these equations, the equations to calculate the different regions of dynamic instability for the different approximations are obtained.

The boundaries for the first region of instability with first order approximation are obtained by solving equation (19). The second order approximation for the boundaries for the same region is given by equation (20).

$$[I] - (P_S \pm \frac{P_d}{2})[K]^{-1}[K_G] - \frac{\theta^2}{4}[K]^{-1}[M] = 0 \qquad (19)$$

$$\begin{vmatrix} [I] - (P_S \pm \frac{P_d}{2})[K]^{-1}[K_G] & -\frac{P_d}{2}[K]^{-1}[K_G] \\ -\frac{P_d}{2}[K]^{-1}[K_G] & [I] - P_S[K]^{-1}[K_G] - \frac{9\theta^2}{4}[K]^{-1}[M] \end{vmatrix} - \theta_2^2 \begin{vmatrix} \frac{1}{4}[K]^{-1}[M] & 0 \\ 0 & 0 \end{vmatrix} = 0 \qquad (20)$$

The boundaries for the second region of instability with first approximation are given by equations (21) and the second approximation for the second region of instability can be obtained from equations (22).

$$[I] - P_S[K]^{-1}[K_G] - \theta^2[K]^{-1}[[M] = 0 \tag{21}$$

$$\begin{vmatrix} [I] - P_S[K]^{-1}[K_G] & -\frac{P_d}{2}[K]^{-1}[K_G] \\ -\frac{P_d}{2}[K]^{-1}[K_G] & [I] - P_S[K]^{-1}[K_G] - 4\theta_1^2[K]^{-1}[M] \end{vmatrix} - \theta_2^2 \begin{vmatrix} [K]^{-1}[M] & 0 \\ 0 & 0 \end{vmatrix} = 0 \tag{22a}$$

$$\begin{vmatrix} [I] - P_S[K]^{-1}[K_G] & -\frac{P_d}{2}[K]^{-1}[K_G] \\ -P_d[K]^{-1}[K_G] & [I] - P_S[K]^{-1}[K_G] \end{vmatrix} - \theta^2 \begin{vmatrix} 0 & 0 \\ 0 & [K]^{-1}[M] \end{vmatrix} = 0 \tag{22b}$$

It is easy to realise that these equations can be solved as eigenvalue problems.

3.1. Results

3.1.1 Isotropic Plate

A analysis of the dynamic instability of an isotropic square plate with Young's modulus of 70GPa, $\rho = 1543\text{Kg/m}$, $\nu = 0.25$, thickness of 3mm and a ratio $a/h = 100$ was performed.

In Figure 1 the results for the first region of instability are presented as a plot of frequency (θ) against β, that is the dynamic load factor used to obtained P_d as a function of the buckling load ($P_d = \beta N_{cr}$).

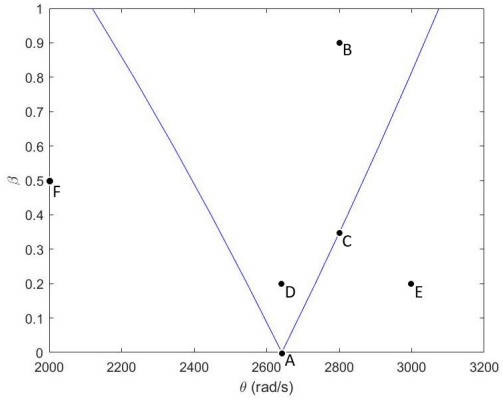

Figure 1: Dynamic instability region for an isotropic plate

To better understand the dynamic instability region and to verify the reliability of those regions, a direct integration using Newmark's Method was performed. The time increment used is $\Delta t = 9 \times 10^{-5}$s. An initial displacement of 0.0012m was imposed to the w_0 degree of freedom on the central node of the plate. The load cases studied are the ones represented in Figure 1. The results for the different points are depicted in Figures 2(a-f).

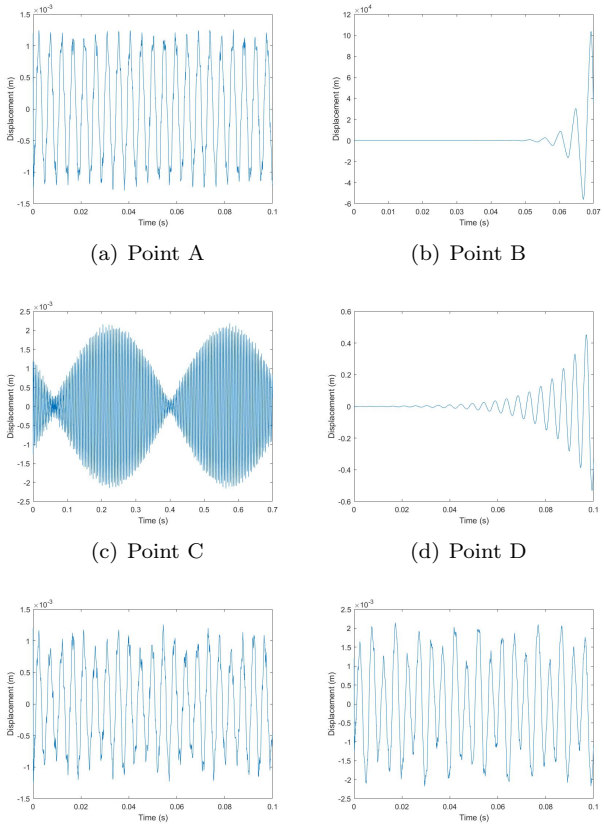

(a) Point A (b) Point B

(c) Point C (d) Point D

(e) Point E (f) Point F

Figure 2: Displacement vs Time diagrams

Figures 2, besides allowing to understand better how the dynamic instability region is translated in the plate behaviour, it also shows that the boundaries obtained are quite good. Points F and E that are in the stable area present, in Figures 2(e) and (f), respectively, a stable behaviour since the amplitude of the displacement is the same trough time. On the other hand, Figures 2(b) and (d) show that the points B and D are, clearly unstable. Both diagrams present an increasing of the amplitude of the displacement with time, which is an unstable behaviour. Finally, Points A and C that are both in the boundary between the stable and unstable region present different behaviours. Figure 2(a) shows that the amplitude of motion is constant. Although, Figure 2(c) depicts a beat-frequency oscillation. This phenomenon happens when the plate vibrates with two different frequencies that interfere with each other. The oscillation amplitudes add or subtract themselves as a result of this discrepancy in vibrational frequencies due to a time variable phase difference between the components of the motion, and the resulting oscillation amplitude takes values between the sum and the difference between the corresponding amplitudes.

Adding equation (20) to the computational process the second approximation for the first region of dynamic instability is obtained. Evolving the analyse, and, also, adding equations (21) and (22), the first and second approximation for the second region of insta-

bility are obtained. Both approximations for the first and second region are shown in Figure (3).

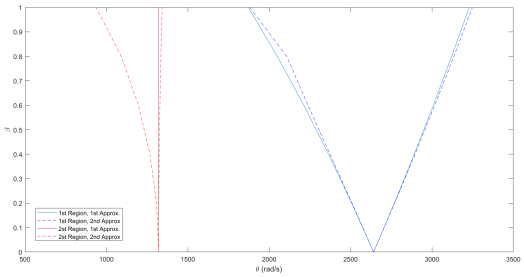

Figure 3: First and second approximation of the first and second dynamic instability region for an isotropic plate

3.1.2 Orthotropic Plate

In the study of the dynamic instability of an orthotropic plate the ply studied was a square plate with $a/h = 100$ and $a = b = 1$m. The material properties are $E_1 = 173$GPa, $E_2 = 33.1$GPa, $G_{12} = 9.38$GPa, $\nu = 0.25$ and density of 1000Kg/m^3.

The results obtained for the principal region of dynamic instability, as a plot of frequency θ against the dynamic load factor β, are shown in Figure 4(a) and 4(b) for the FSDT and HSDT model, respectively.

The dimensions of the plate will affect deeply the location of the dynamic instability region. One important factor that will have an impact is the thickness of the plate. In order to analyse its impact a dynamic instability analysis was performed for the orthotropic plate already studied with different ratios b/h. The results obtained are presented in Figure 5. These results allow to conclude that the ratio b/h has a great impact on the location of the principal dynamic instability region. The increase of b/h, meaning the decrease of the thickness, shifts the principal dynamic instability region to the left. So thicker plates have the instability regions in a zone of higher frequencies. The results, also, shows that the difference is considerable since the difference on the frequencies of the boundaries are, sometimes, of some thousand rad/s.

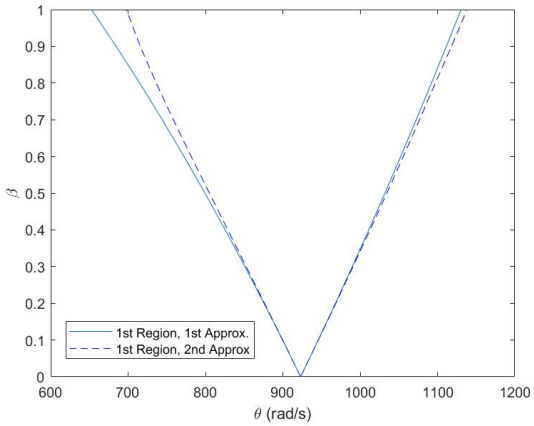

(a) using FSDT model

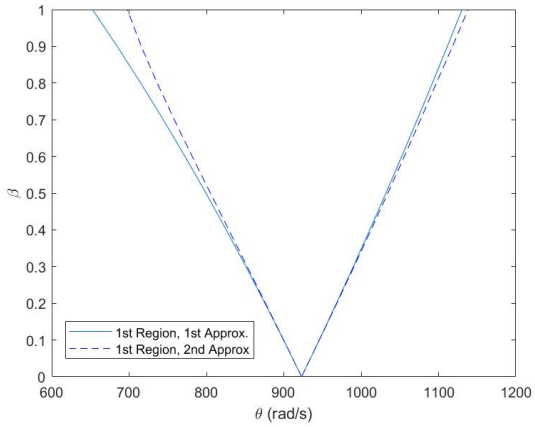

(b) using HSDT model

Figure 4: First and second approximation to principal region of dynamic instability for a square orthotropic plate

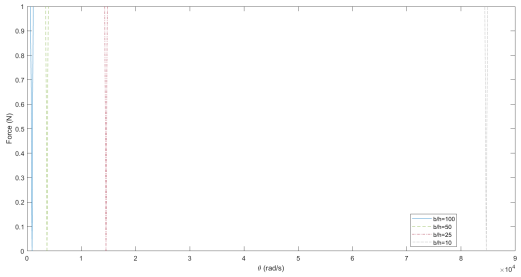

Figure 5: First dynamic instability region for different values of b/h

3.1.3 Laminated Composite Plates

In this section, a four layer cross-ply laminated plate is analysed. Each ply has the same thickness and is a square plate with a $[0°/90°/90°/0°]$ lay up, a ratio of $a/h = 25$ and $a = 10\text{in} = 0.254\text{m}$. Each ply was made of the same orthotropic material, which have the following mechanical properties: $E_2 = 10^6\text{lb/in}^2 = 6.8948\text{GPa}$, $E_1 = 40E_2$, $G_{12}/E_2 = G_{13}/E_2 = 0.6$, $G_{23}/E_2 = 0.5$, $\nu_{12} = 0.25$ and $\rho = 1\text{lbs}^2/\text{in}^4 = 1.06864 \times 10^7\text{Kg/m}^3$.

Figure 6(a) and 6(b) depict, both approximations, of the principal dynamic instability region for the FSDT and HSDT model, respectively. The results are plotted as frequency θ (rad/s) against the dynamic load factor β.

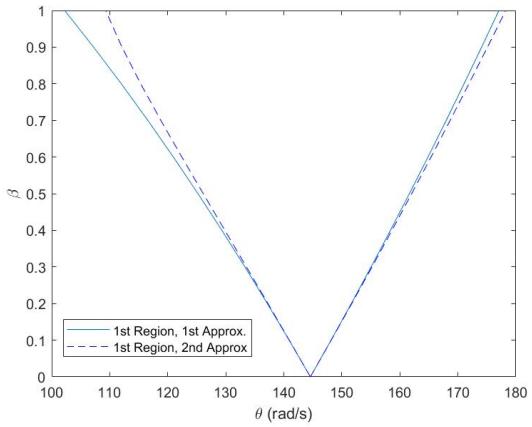

(a) using FSDT model

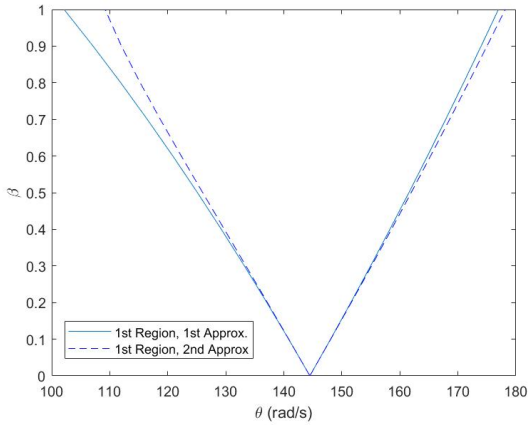

(b) using HSDT model

Figure 6: First and second approximation to principal region of dynamic instability for a four layered cross-ply laminated plate

In order to understand how the ratio a/b affects the dynamic instability of a composite laminated plate a parametric study was performed. Analysing the same laminated composite plate already used in this section, but varying its relation a/b, the principal dynamic instability regions presented in Figure 7, were obtained.

This parametric study show how the ratio a/b affects the dynamic instability region of a composite laminated plate. The results presented in Figure 7 permit to conclude that the increase of a/b shifts the dynamic instability zone to the right, meaning to a zone with higher frequencies. The difference becomes less significant for higher ratios a/b and vice versa. The width of the region tends to decrease with the increase of a/b and, consequently, the area of the unstable dynamic region decreases with the increase of a/b.

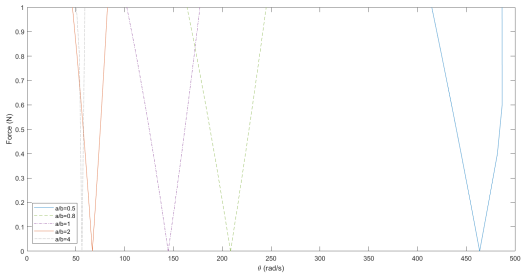

Figure 7: First dynamic instability region for different values of a/b

Figures 4 and 6 shows that both theories, FSDT and HSDT, presented really similar results for the frequencies of the boundaries of the instability dynamic region. It is even possible to say that, in general, the results are the same for both theories. Since FSDT needs a smaller computational effort it was the theory used to perform the parametric analysis presented.

4. Sandwich Plates

4.1. Sandwich Plates

A sandwich panel generally consists of two thin but stiff face sheets or skins separated by a light-weight and thick but low modulus core [10]. The face sheets are usually laminated composite materials, but, can also be made of metallic materials. Moreover, the core is usually made of a light-weight material, such as, a foam polymer or a honeycomb material. The main objective of the core, in a sandwich plate, is to reduce the weight of the structure while producing a high resistance to transverse loads or damping unwanted vibrations.

4.1.1 Numerical Model

The model formulates the sandwich panel as two laminated composite plates (e_1, e_2) and an elastic core (c) between them. Figure 8 is a visual representation of the model developed. The two laminated composite layers (e_1, e_2) are modelled using the first shear deformation theory, while the core (c) is modelled with the higher-order shear deformation theory.

Adapting equations (3) for the laminated composite plates (e_1, e_2), the displacement field for these layers is given, in the general form, by equations (23), where $i = e_1, e_2$ and z_i is obtained by equation (24).

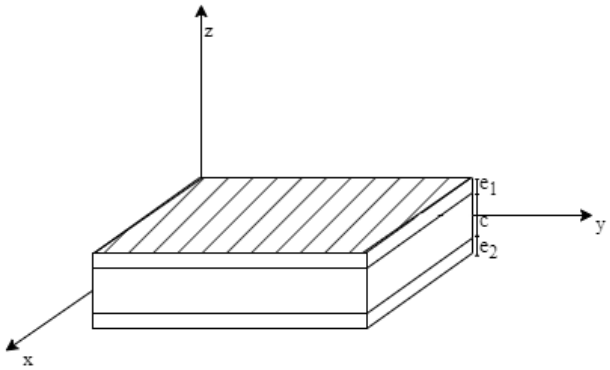

Figure 8: Sandwich plate model

$$u^i(x,y,z,t) = u_0^i(x,y,t) + (z - z_i)\,\theta_x^i(x,y,t) \quad (23a)$$

$$v^i(x,y,z,t) = v_0^i(x,y,t) + (z - z_i)\,\theta_y^i(x,y,t) \quad (23b)$$

$$w^i(x,y,z,t) = w_0^i(x,y,t) \quad (23c)$$

$$z_{e_1} = \frac{h_c}{2} + \frac{h_{e_1}}{2}, \qquad z_{e_2} = -\frac{h_c}{2} - \frac{h_{e_2}}{2} \quad (24)$$

Since the core is modelled with the HSDT, the displacement field is given adapting equation (4) and can be written as:

$$u_c(x,y,z,t) = u_0^c(x,y,t) + z\theta_x^c(x,y,t) + z^2 u_0^{*c}(x,y,t) + z^3\theta_x^{*c}(x,y,t) \quad (25a)$$

$$v^c(x,y,z,t) = v_0^c(x,y,t) + z\theta_y^c(x,y,t) + z^2 v_0^{*c}(x,y,t) + z^3\theta_y^{*c}(x,y,t) \quad (25b)$$

$$w^c(x,y,z,t) = w_0^c(x,y,t) + z\theta_z^c(x,y,t) + z^2 w_0^{*c}(x,y,t) \quad (25c)$$

4.1.2 Dynamic Instability Analysis

A plate that consists of laminated cross ply face sheets and an isotropic core with a [0°/90°/core/90°/0°] lay up is analysed. Each of the face sheet plies is assumed to be the same thickness, the ratio between the thickness of the core and the total thickness (h_c/h) is taken to be 0.8, being the total thickness 1mm, and the ratio a/h is 10. The properties of the materials used for the face sheets and the core are the following:

- Face sheets: $E_1 = 276$GPa, $E_2 = G_{12} = G_{13} = G_{23} = 10.34$GPa, $\nu_{12} = 0.22$ and $\rho = 681.8$Kg/m^3;
- $E_1 = E_2 = 0.5776$GPa, $G_{12} = G_{13} = 0.1079$GPa, $G_{23} = 0.22215$GPa, $\nu_{12} = 0.0025$ and $\rho = 1000$Kg/m^3.

Figure 9 depicts the first and second approximations for both, the first and second dynamic instability regions, for the plate under analysis.

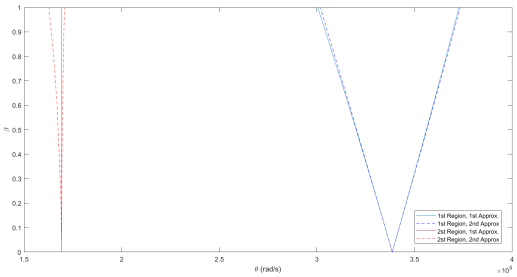

Figure 9: First and second approximation of the first and second dynamic instability region for a symmetric sandwich plate

The core and its dimensions is a relevant part of a sandwich plate and it will have an important impact on the mechanical behaviour of the plate. In order to study the influence of the thickness of the core on the dynamic instability of a sandwich plate, the principal dynamic instability region was obtained, for the sandwich plate already studied in this section, for different values of h_c/h. Figure 10 depicts the results obtained. These results shows that the decrease of the ratio h_c/h shifts the principal dynamic instability region to the right. This means that sandwich plates with thicker cores will have the principal dynamic instability region for lower frequencies and vice versa.

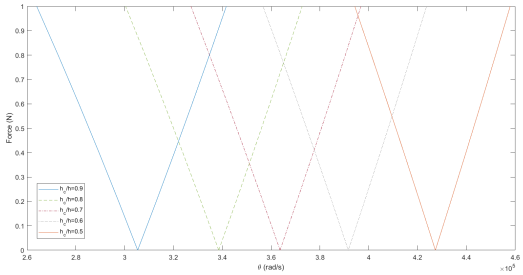

Figure 10: First dynamic instability region for different values of h_c/h

4.2. Sandwich Plates with Viscoelastic Core

Viscoelastic materials are frequently employed as core materials where damping is a major concern because they undergo significant deformations under external pressure and have the capacity to absorb and dissipate energy. They have characteristics of both viscous and elastic materials. The damping effect can be added to the model in different ways. In this work it is going to be used two different types of damping, proportional damping and hysteretic damping, using complex variables.

4.2.1 Numerical Model

Proportional Damping

To the equation of motion of a plate, already shown on equation (14), can be added a damping term and it would be given by:

$$[M]\{\ddot{x}\} + [C]\{\dot{x}\} + [K]\{x\} - P(t)[K_G]\{x\} = 0 \quad (26)$$

where [C] is the damping matrix in the form $[C] = \alpha[M] + \beta[K]$ but, during the development of this work, $\beta = 0$ was considered. If the damping coefficient (ϵ) is given by $\epsilon = \alpha/2$, equation 26 present the form show in equation 27, when the solutions wanted are in the form $x = e^{-\epsilon t}u(t)$ and $e^{\epsilon t}$ is not singular.

$$[K]^{-1}[M]\{\ddot{u}\} + \{[I] - [K]^{-1}[M]\epsilon^2 - [P_s + P_d\phi(t)]\,[K]^{-1}[K_G]\}\{u\} = 0 \quad (27)$$

The boundary frequency equations can be found by looking for periodic solutions, such as the Fourier series represented by equations (15) and (16), which, when inserted into equation (26), offer two linear homogeneous systems with approximate solutions. Equation (28) presents the system to obtained solutions with a period of 2T.

$$\begin{vmatrix} [I] - (P_S + \frac{P_d}{2})[K]^{-1}[K_G] - \frac{\theta^2}{4}[K]^{-1}[M] & -\theta[K]^{-1}[M]\epsilon \\ \theta[K]^{-1}[M]\epsilon & [I] - (P_S + \frac{P_d}{2})[K]^{-1}[K_G] - \frac{\theta^2}{4}[K]^{-1}[M] \end{vmatrix} = 0 \quad (28)$$

Hysteretic Damping

As already mentioned, the hysteretic damping can be added to the system through the use of complex variable. The shear modulus of viscoelastic materials is expressed in complex form as $G = G' + iG''$, where G' and G" are the real part and imaginary part of the complex modulus and are measures of the total energy stored and dissipated, respectively.

In this work to modelled a sandwich plate with viscoelastic core was used the model already presented in section 4.1.1, giving complex values for the Young's modulus. Then E can be written as:

$$E_c = E' + \eta E' i \quad (29)$$

where η is the material loss factor. The analysis performed was done using the exactly same model presented in sections 3 to obtained the dynamic instability regions. The results obtained from the eigenvalue problems will be, obviously, complex and it will be needed to calculated their modulus to obtained the final result.

For sandwich plates with a viscoelastic core the vibration characteristics are usually associated with the modal loss factor. The measure of the vibratory energy absorbed by the structure is represented by the modal loss factors, which are the normalised imaginary portions of the bending stiffness. The modal loss factor can be calculated by:

$$\eta_i = \frac{\omega_I}{\omega_R} \quad (30)$$

where i indicates the mode, ω_I is the imaginary component of ω and ω_R is the real part.

4.2.2 Dynamic Instability

To analyse the effects of adding a viscoelastic core to a sandwich plate the same plate was studied for both methods. The plate under analysis is a square, three layered sandwich plate with a [0°/core/0°] lay-up, thickness of 1mm and $a/h = 100$. The mechanical properties of the isotropic materials that the face sheet and the core are made of are the following:

- Face sheets: $E_f = 66$GPa, $\nu_{12} = 0.33$ and $\rho_f = 2680$Kg/m^3;
- Core: $E_c = 5.2 + x5.2i$MPa, $\nu_{12} = 0.3$ and $\rho_c = 1015$Kg/m^3.

Proportional Damping

Figure 11 depicts the principal dynamic instability region for the sandwich plate with $\alpha = 0$, meaning that it should behave like a system without damping, therefore without a viscoelastic core. Whereas, Figure 12 presents the same region for a sandwich plate with a viscoelastic core with $\alpha = 50$.

In order to analyse the effect that damping has on the behaviour of the plate over time a direct integration using Newmark's Method was performed. The time increment used was $\Delta t = 0.00008$s and an initial displacement of 0.0004m was imposed to the w_0 degree of freedom on the central node of the plate. A group of the same load cases were studied for both plates to better compare the damping effect on different regions. Figures 13(a-d) depict the time vs. displacement diagrams for the load cases for $\alpha = 0$ and Figures 14(a-d) for $\alpha = 50$.

Figures 13(a-d) and 14(a-d) are a good way to check the reliability of the regions obtained. Figures 13 depict the expected diagrams for a system with no damping where the points outside the dynamic instability region will show a stable behaviour in which the amplitude keeps the same over time, and the points inside the unstable region present an increase of the amplitude with time. Relevant to mention, that this increase becomes more sensitive when the point is further away from the boundaries. On the other side, Figures 14 depict a very different behaviour. Figures 14(a), 14(b) and 14(c) are characterised by a displacement function whose amplitude decreases exponentially with time. Since the point C' is in the boundary between regions or really close to it, it shows a softer damping where the decrease of amplitude is slower than the others. Figure 14(d) shows a typical unstable behaviour which was the expected result since point D' is in the unstable region.

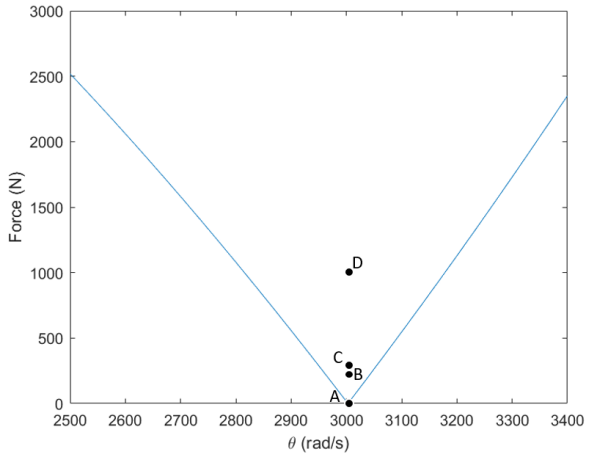

Figure 11: Principal dynamic instability region for $\alpha = 0$

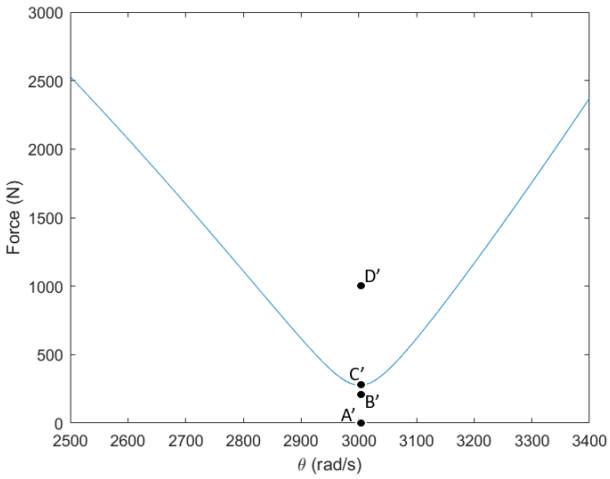

Figure 12: Principal dynamic instability region for $\alpha = 50$

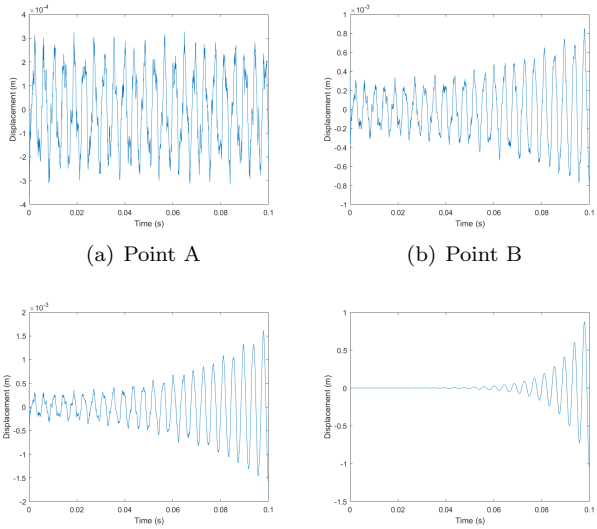

(a) Point A (b) Point B

(c) Point C (d) Point D

Figure 13: Displacement vs Time diagrams of a sandwich plate with viscoelastic core with $\alpha = 0$

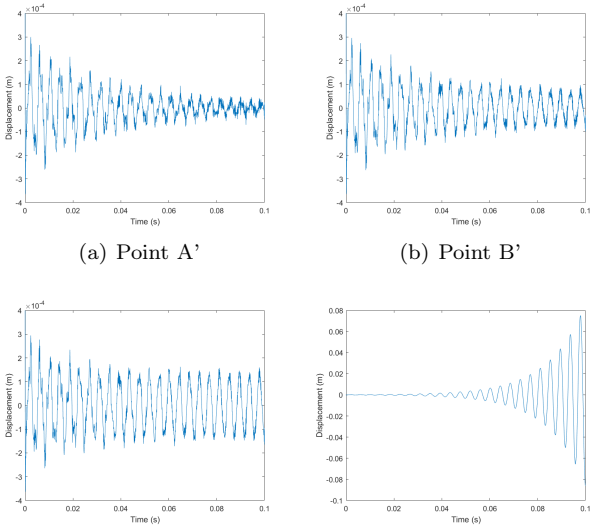

(a) Point A' (b) Point B'

(c) Point C' (d) Point D'

Figure 14: Displacement vs Time diagrams of a sandwich plate with viscoelastic core with $\alpha = 50$

To study the effect of α on the mechanical behaviour and, consequently, on the dynamic instability regions of a sandwich plate with a viscoelastic core, a dynamic instability analysis to plates with different values of α were performed. The results can be seen in Figure 15 which depicts the different dynamic instability principal regions.

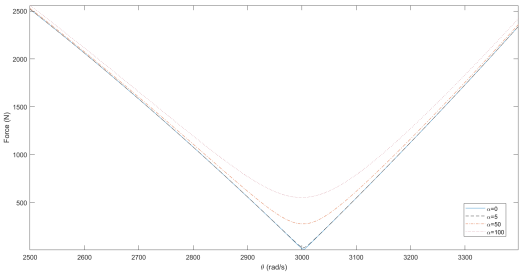

Figure 15: Principal dynamic instability region of a sandwich plate with viscoelastic core for different α

Hysteretic Damping

A dynamic stability analysis,using the hysteretic damping model, was performed on the sandwich plate with a viscoelastic core. Figure 16 depicts the principal dynamic instability region for multiple values of η.

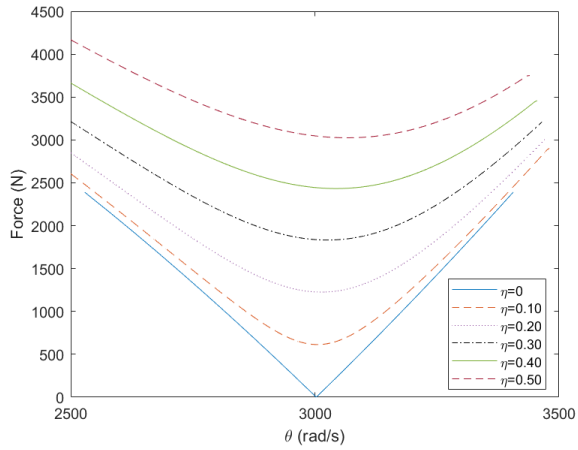

Figure 16: Principal dynamic instability region of a sandwich plate with viscoelastic core for different η

From the results presented, it is possible to conclude that adding a viscoelastic core to a sandwich plate will add damping to the system. Damping will transform the dynamic instability region. The minimum will present a round shape instead of a peak and that minimum is for a dynamic force applied to the system bigger than 0.

5. Conclusions

The work developed in this thesis allowed to enlarge the computationally efficient finite element models already developed in Matlab by Tomé[7]. It added two more analysis, a free vibration analysis and a dynamic instability analysis, with and without damping.

The numerical model used to study the dynamic instability of the structures analysed was developed. This model was applied to isotropic, orthotropic and laminated composite plates. Different studies were made, showing how various parameters might affect the dynamic instability of the plates analysed. These parametric studies covered the changes in parameters like the ratios b/h and a/b.

The sandwich plate model was formulated with the face sheets based on the FSDT and the core based on the HSDT. The dynamic instability model was, also, applied to a sandwich plate. The results obtained validate, once again, the models used and that the generated Matlab code is working as planned and delivering satisfactory results. One more parametric study was performed. This time was to analyse the impact that the thickness of the core has in the dynamic answer of the system. Two different models to add the damping from the viscoelastic core to the sandwich plate system were developed, one with proportional damping and the other with hysterical damping. The results obtained were in accordance with what was expected.

Developments and extensions of the present work can be done trough multiple ways. Some relevant ideas, but not exclusively, are adding piezoelectric sensors and actuators to the model and studied their effect in the dynamic instability or validate the results obtained in the present work trough experimental studies.

Acknowledgements

The author would like to thank Prof. Aurélio Araújo for all the support given.

References

[1] Charles A. Osheku. *Lamination*. IntechOpen, Mar 2018.

[2] Aneta Krzyzak, Michał Mazur, Mateusz Gajewski, Kazimierz Drozd, Andrzej Komorek, and Paweł Przybyłek. Sandwich structured composites for aeronautics: Methods of manufacturing affecting some mechanical properties. *International Journal of Aerospace Engineering*, 2016, 2016.

[3] M.M. Kheirikhah, S.M.R. Khalili, and K. Malekzadeh Fard. Biaxial buckling analysis of soft-core composite sandwich plates using improved high-order theory. *European Journal of Mechanics - A/Solids*, 31(1):54–66, 2012.

[4] Mohammad R. PERMOON and Touraj FARSADI. Free vibration of three-layer sandwich plate with viscoelastic core modelled with fractional theory. *Mechanics Research Communications*, 116, 2021.

[5] L. S. Ramachandra and Sarat Kumar Panda. Dynamic instability of composite plates subjected to non-uniform in-plane loads. *Journal of Sound and Vibration*, 331:53–65, 1 2012.

[6] A.L. Araújo, V.S. Carvalho, C.M. Mota Soares, J. Belinha, and A.J.M. Ferreira. Vibration analysis of laminated soft core sandwich plates with piezoelectric sensors and actuators. *Composite Structures*, 151:91–98, 2016.

[7] Marta Filipa Abreu Tomé. Buckling analysis of laminated composite and sandwich plates considering the piezoelectric effect. Master's thesis, Instituto Superior Técnico, October 2021.

[8] J. N. Reddy. *Mechanics of laminated composite plates and shells : theory and analysis*. Boca Raton : CRC Press, 2nd edition, 2004.

[9] V. V. Bolotin. *The Dynamic Stability of Elastic Systems*. HOLDEN-DA Y, INC., 1964.

[10] Ali Tian, Renchuan Ye, and Yiming Chen. A new higher order analysis model for sandwich plates with flexible core. *Journal of Composite Materials*, 50:949–961, 3 2016.